2005

The Impact of Non-Stationarities in the Climate System on the Definition of "A Normal Wind Year": A Case Study from the Baltic

S C. Pryor
Indiana State University Bloomington

R J. Barthelmie
Risoe National Laboratory

Justin T. Schoof
Southern Illinois University Carbondale, jschoof@siu.edu

Copyright 2005 Royal Meteorological Society. International Journal of Climatology 25: 735–752 (2005). Published online 26 April 2005 in Wiley InterScience (www.interscience.wiley.com). DOI: 10.1002/joc.1151

INTERNATIONAL JOURNAL OF CLIMATOLOGY
Int. J. Climatol. **25**: 735–752 (2005)
Published online 26 April 2005 in Wiley InterScience (www.interscience.wiley.com). DOI: 10.1002/joc.1151

THE IMPACT OF NON-STATIONARITIES IN THE CLIMATE SYSTEM ON THE DEFINITION OF 'A NORMAL WIND YEAR': A CASE STUDY FROM THE BALTIC

S. C. PRYOR,[a,b,*] R. J. BARTHELMIE[b] and J. T. SCHOOF[a]

[a] *Atmospheric Science Program, Department of Geography, Indiana University, 701 E. Kirkwood Avenue, Bloomington, IN 47405, USA*
[b] *Department of Wind Energy, Risoe National Laboratory, Dk 4000 Roskilde, Denmark*

Received 4 February 2004
Revised 24 November 2004
Accepted 24 November 2004

ABSTRACT

Wind speeds over the Baltic significantly increased over the second half of the 20th century (C20th), with the majority of the increase being focused on the upper quartile of the wind speed distribution and in the southwest of the region. These changes have potentially profound implications for the wind energy resource. For example, based on the National Centers for Environmental Prediction–National Center for Atmospheric Research (NCEP–NCAR) reanalysis data it is shown that, owing to this non-stationarity, using the normalization period of 1987–98 to determine the wind resource (as in the Danish wind index) leads to overestimation of the wind energy index (and hence the wind energy resource) in western Denmark relative to 1958–2001 by approximately 10%. To address whether the increased prevalence of high wind speeds at the end of the C20th will be maintained in the future, we provide a first prognosis of annual wind indices from the HadCM3 coupled atmosphere–ocean general circulation model. The results suggest the 21st century (C21st) will be similar to the 1958–2001 period with respect to the wind energy density, but that the northeastern Baltic will exhibit slightly higher wind energy indices over the course of the C21st relative to the latter half of the C20th, whereas the southwest of the Baltic exhibits some evidence of declining wind indices towards the end of the C21st. These changes may indicate a tendency in HadCM3 towards more northerly tracking of mid-latitude cyclones in the future, possibly due to evolution of the North Atlantic oscillation. As a caveat to this finding, it should be noted that the NCEP–NCAR and European Centre for Medium-Range Weather Forecasts reanalysis data sets and HadCM3 simulations, although exhibiting commonalities during the period of overlap, differ quantitatively in terms of the spatial fields and empirical cumulative probability distributions at individual grid cells. Copyright © 2005 Royal Meteorological Society.

KEY WORDS: wind index; climate change; prognoses; trends; reanalysis data; general circulation models

1. INTRODUCTION

1.1. Background

In the context of wind energy applications, where wind farms have typical lifetimes of the order of 30 years, the question that is often asked is 'What is a *normal wind year*?', or alternatively stated, 'Over the lifetime of the wind farm what is the average expected energy production?' Recall energy density is $1/2\rho U^3$, and hence the cumulative annual energy density is dominated by the upper percentiles of the wind speed cumulative probability distribution. The question stated above can be extended to encompass the following: 'Will non-stationarities in the global climate system cause the definition or magnitude of a *normal wind year* to evolve on time scales of relevance to wind energy developments?' The research presented herein is a first attempt to address this question in the context of the Baltic Sea region using historical observations

* Correspondence to: S. C. Pryor, Atmospheric Science Program, Department of Geography, Indiana University, 701 E. Kirkwood Avenue, Bloomington, IN 47405, USA; e-mail: spryor@indiana.edu

from reanalysis data sets and projected flow regimes from a coupled atmosphere–ocean general circulation model (AOGCM). Most previous research in this field has focused on downscaling procedures of potential future flow climates (Mengelkamp, 1999; Sailor *et al*., 2000). The research presented here adopts a different approach to development of projected wind climates and energy density. It additionally provides context by addressing concerns regarding the realism of near-surface flow regimes within AOGCMs and the magnitude of differences between AOGCM simulations of current climate and those from reanalysis data sets relative to differences between projected and current wind speed regimes.

1.2. Recent climate variability in the Baltic basin

The study region is the Baltic basin and extends from approximately 52.5 °N, 3.75 °E to 65 °N, 26.5 °E (Figure 1). The climate of the Baltic is dominated by the passage of cyclones and, in agreement with studies that indicate coherent variations in the frequency and intensity of transient eddies in the Northern Hemisphere middle latitudes (Serreze *et al*., 1997; Ulbrich and Christoph, 1999; Geng and Sugi 2001), the annual mean wind speed at 850 hPa over the Baltic as manifest in the National Centers for Environmental Prediction–National Center for Atmospheric Research (NCEP–NCAR) reanalysis project significantly increased over the period 1953–99, particularly in the southwest of the region (Pryor and Barthelmie, 2003). The majority of the wind speed increase was focused on the upper quartile of the wind speed distribution and, hence, has implications for wind energy. These changes in wind speed are strongly linked to variations in the synoptic-scale circulation (Pryor and Barthelmie, 2003) as manifest in the Grosswetterlagen catalogue (Gerstengarbe and Werner, 1999) and the recent prevalence of the positive phase of the North Atlantic oscillation (NAO; Greatbach, 2000; Hastenrath and Greischar, 2001; Marshall *et al*., 2001). Here, we extend this work by assessing whether these wind speed trends are also evident at other levels in the atmosphere and in another (independent) reanalysis data set, and by providing an analysis of projected changes from an AOGCM simulation.

1.3. Objectives

The objectives of the research presented here are to:

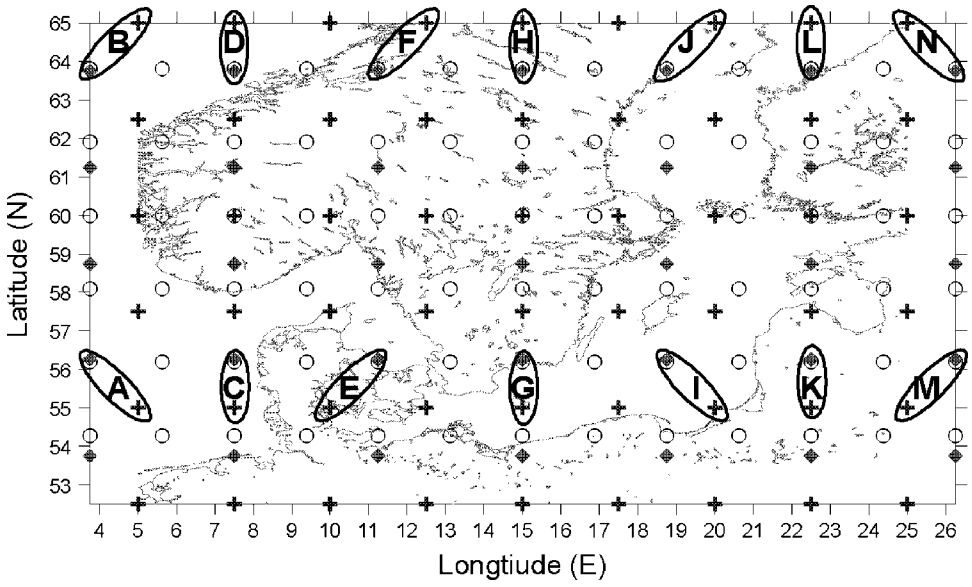

Figure 1. Map of the study region showing the grid point locations for the NCEP–NCAR reanalysis data (○), the ECMWF reanalysis data (+), and HadCM3 (♦). The grid cells referred to specifically in the text are labelled with the characters used in Table I

1. Quantify the degree of interannual variability of the wind speed and wind energy density in the historical record for the 20th century (C20th) from the Baltic basin. Specifically, we quantify temporal variability and trends in flow regimes and wind energy availability within the last 50 years in two reanalysis data sets. A related objective is to compare and contrast the magnitude of spatial and temporal variability in near-surface wind speeds from these two independent data sets.
2. Determine the degree to which an AOGCM captures recent spatio-temporal variability of recent wind speeds in the Baltic and to extrapolate wind indices for the 21st century (C21st).

2. DATA

2.1. Reanalysis data

Reanalysis projects, such as those developed at NCEP–NCAR (Kalnay *et al*., 1996; Kistler *et al*., 2001) and the European Centre for Medium-Renge Weather Forecasts (ECMWF; Simmons and Gibson, 2000), draw data from a range of sources; these data are quality controlled and assimilated with a consistent data simulation system (model). These reanalysis products thus comprise four-dimensional, homogenized and systematic data sets. With regard to the current analysis, it is worth noting that neither project assimilates observations of 10 m wind speeds over land, but both assimilate 10 m wind speeds as derived from satellite-borne scatterometer instrumentation.

In this analysis we use 10 m wind speeds because, of the flow levels archived for AOGCMs, it most closely approximates the flow that influences wind energy resources. Additionally, we focus on wind speeds in grid cells that are spatially coincident or nearly so between the two reanalysis data sets and HadCM3 (see Table I) and specifically on three sample grid cells. Grid cell C, in the southwest of the domain, west of Denmark, is a region of mixed land–sea surface. Grid cell I is over the interior of the Baltic Sea and, hence, contains predominantly water surfaces. Grid cell L is located in the northeast of the domain over the Finnish coastline (see Figure 1). Although the grid cells highlighted in Table I show some overlap, it should be noted that the degree of correspondence is higher for grid cell centroids from the NCEP–NCAR reanalysis and HadCM3 than between the ECMWF reanalysis and either of the other two model data sets.

Table I. The location of the coincident grid cells from the reanalysis data sets and HadCM3. The two right-hand columns show the 'trend' term m in regression Equation (9) of the annual 90th percentile wind speeds. Values are only shown if the 95% confidence intervals on the trend term did not include zero

	ECMWF		NCEP/NCAR		HadCM3		Trend analysis	
Grid cell	Lat (°N)	Long (°E)	Lat (°N)	Long (°E)	Lat (°N)	Long (°E)	NCEP–NCAR	ECMWF
A	55	5	56.1893	3.75	56.25	3.75	0.036	0.032
B	65	5	63.8081	3.75	63.75	3.75	0.029	—
C	55	7.5	56.1893	7.5	56.25	7.5	0.029	0.026
D	65	7.5	63.8081	7.5	63.75	7.5	0.028	0.018
E	55	10	56.1893	11.25	56.25	11.25	0.018	0.013
F	65	10	63.8081	11.25	63.75	11.25	0.011	0.017
G	55	15	56.1893	15	56.25	15	0.013	0.015
H	65	15	63.8081	15	63.75	15	0.009	—
I	55	20	56.1893	18.75	56.25	18.75	0.019	—
J	65	20	63.8081	18.75	63.75	18.75	—	—
K	55	22.5	56.1893	22.5	56.25	22.5	0.011	—
L	65	22.5	63.8081	22.5	63.75	22.5	—	—
M	55	25	56.1893	26.25	56.25	26.25	—	—
N	65	25	63.8081	26.25	63.75	26.25	—	—

2.1.1. The NCEP–NCAR reanalysis project. The NCEP–NCAR reanalysis data are available from 1948. Herein we use four-times daily (00, 06, 12, 18 UTC) 10 m wind speeds calculated from the data set wind components (u and v) for each $1.875^\circ \times 1.875^\circ$ grid shown in Figure 1 for the period 1958 to 2001. The atmospheric model used for the NCEP–NCAR reanalysis project is spectral (horizontal resolution: T62 which is roughly equivalent to a horizontal resolution of 210×210 km^2) with transformation to a Gaussian grid for calculation of nonlinear quantities and physics. The vertical domain is divided into 28 unequally spaced sigma levels with enhanced resolution near the bottom and the top.

2.1.2. The ECMWF reanalysis project. The new reanalysis project at ECMWF (ERA-40) covers the period from mid-1957. Herein, we use four-times daily (00, 06, 12, 18 UTC) 10 m wind speeds and direction calculated from the data set wind components (u and v) for each $2.5^\circ \times 2.5^\circ$ grid shown in Figure 1 for the period 1958–2001 inclusive. The atmospheric model used for ERA-40 also uses a spherical-harmonic representation for basic dynamic fields, with a reduced Gaussian grid of approximately uniform 125 km spacing for surface and other grid-point fields.

2.2. General circulation model: HadCM3

In this preliminary analysis we use daily output from the HadCM3 coupled AOGCM (Johns *et al*., 1997; Stratton, 1999; Pope *et al*., 2000) for the transient simulation (1990–2099) under the Intergovernmental Panel on Climate Change's (IPCC's) *Special Report on Emissions Scenarios* (SRES) A2 emission scenario (Nakicenovic and Swart, 2000). HadCM3 is a Cartesian model. The atmospheric component of HadCM3 has 19 levels, and a horizontal resolution of 2.5° latitude by 3.75° of longitude (Figure 1), which produces a global grid of 96×73 grid cells. This is equivalent to a surface resolution of about 417 km $\times$ 278 km at the equator, reducing to 295 km $\times$ 278 km at 45° latitude (comparable to a spectral resolution of T42). The oceanic component of HadCM3 has 20 levels and a horizontal resolution of $1.25^\circ \times 1.25^\circ$.

The SRES's scenarios, as developed by the IPCC, encompass a range of parameters that dictate emissions, including demographic, technological and economic changes. The SRES A2 scenario provided one of the foci of the model intercomparison research presented in Houghton *et al*. (2001), and equates to a moderate to high greenhouse gas cumulative emission for 1990 to 2100 as a result of projected population growth and fairly slow introduction of alternative technologies. This scenario results in global carbon dioxide (CO_2) emissions from industry and energy in 2100 that are almost four times the 1900 value and by 2100 the emissions from land-use change are close to zero, leading to a global CO_2 emission (as carbon) in 2100 of almost 28 GtC year^{-1}. The global temperature increase simulated by HadCM3 for this emission scenario is approximately equal to $+4\,^\circ$C from 1960 to 2100. The A2 emissions scenario is used in this analysis to provide a reasonable upper bound on likely climate change and hence a high signal-to-noise ratio when comparing current with future flow climates.

2.3. Wind indices

Wind energy indices are simple mechanisms for assessing inter- and intra-annual variability of wind energy and are often used to provide a context for shorter term, site-specific time series measured by wind-energy developers to assess the feasibility of wind-farm installations. The Danish wind energy index thus provides a regional assessment of monthly and annual variability of observed wind energy normalized to the 12-year data period 1987 to 1998 (see www.emd.dk). The index as used here is

$$\text{Index} = \overline{\sum_{j=1}^{n} \frac{U_j^3}{U_{i,\ldots,k}^3}} \times 100 \tag{1}$$

where $j = 1, \ldots, n$ indicates the time series from the period of interest and $i, \ldots, k$ indicates the normalization period. Wind indices exhibit intra- and inter-annual variability and, naturally, the index for any given year is determined in part by the normalization period used.

AOGCMs are most accurate at large spatial and temporal scales (Houghton *et al.*, 2001), and there is evidence of bias in HadCM3 wind speeds relative to observations (see Section 4). Wind indices are thus used herein, because the normalization inherent in calculation of wind indices reduces the impact of offsets in wind speeds simulated by AOGCMs. However, the accuracy of the wind indices is dependent on the accuracy with which any model represents the variability and range of wind speeds.

3. HISTORICAL WIND CLIMATE FOR THE BALTIC

3.1. Non-stationarities in the wind climate: the influence of normalization period on the wind index

3.1.1. Methods. We examine the sensitivity of a wind index calculated using Equation (1) to assumptions regarding the period used for normalization using the two reanalysis data sets. Wind indices are calculated for 12-year moving windows for each grid cell such that for each grid cell and year there are 33 realizations of the index corresponding to the 33 12-year normalization periods between 1958 and 2001.

3.1.2. Results. Figure 2 shows the mean annual wind index for 1958–2001 calculated from the ECMWF and NCEP–NCAR reanalysis data for grid cells C, I and L presented as a function of the normalization period. Owing to the relatively low wind speeds during the late 1950s to 1970, mean wind indices for these grid cells calculated using the beginning of the record as the normalization interval exhibit values above 100%, whereas the converse is true for the normalization by the latter portion of the period. For example, using the 1987–98 data for the normalization gives a mean annual wind index for grid cell C over 1958–2001 of 88–92%. This may be interpreted as indicating that the mean wind energy resource over western Denmark for 1958–2001 is approximately 10% lower than that during the period 1987–98. For the other two grid cells shown in Figure 2, the 1987–98 period also exhibited higher average wind energy density than was typical of 1958–2001. For grid cell L the maximum in wind indices was observed for normalization periods focused on the late 1970s and early 1980s. This indicates that, in contrast to the more southerly grid cells, both the late 1950s–1970 and the late 1970s–1980s were characterized by atypically low wind energy in the northeast of the domain. In summary, for the grid cells considered here, 1987–98 does not represent a robust wind energy climatology relative to the entire period of 1958–2001, whereas for the three grid cells shown in Figure 2, based on data from the NCEP–NCAR reanalysis, 1970–81 is arguably the 12 year period that best represents the 1958–2001 period. Discrepancies between the reanalysis data sets as evident in Figure 2 are considered in more detail in the following section.

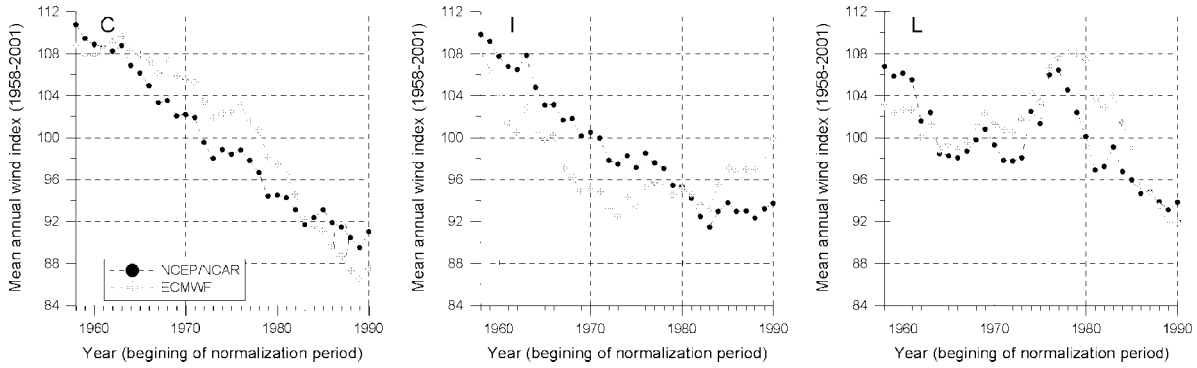

Figure 2. Mean annual wind index for data from 1958–2001 and grid cells C, I and L from the NCEP–NCAR and ECMWF reanalysis data sets presented as a function of the normalization period (plotted at the year which begins the normalization interval). The results for the calculation where the normalization period is 1987–98 are circled in the frame showing grid cell C

3.2. Analysis and comparison of the reanalysis data sets

3.2.1. Methods. Reanalysis data sets possess some limitations and artifacts (Kistler *et al*., 2001). For example, introduction of satellite-derived observations into the NCEP–NCAR reanalysis assimilation (starting in 1979) generally improved the model performance, but led to some discontinuities in some of the derived fields. Although these discontinuities are most pronounced in the Southern Hemisphere (Kistler *et al*., 2001) and at higher altitudes (Trenberth and Stepanik, 2002), changes in the number and nature of data sets assimilated by the reanalysis process will inevitably lead to some temporal inconsistencies. Hence, despite the clear utility of the reanalysis data sets, there is a recognized need to evaluate the reanalysis projects relative both to other reanalysis data sets and to independent data not assimilated within the reanalysis process (Hines *et al*., 2000; Hastenrath and Greischar, 2001; Smith *et al*., 2001; Marshall, 2002; Schoof and Pryor, 2003). This comparison is particularly relevant to the current application because, as described above, observations of near-surface winds over land are not assimilated by either the ECMWF or the NCEP–NCAR reanalysis models (Kalnay and Cai, 2003). Also, analyses by Frank and Mann (2001) suggest that surface roughness values from Denmark as used in the NCEP–NCAR reanalysis model (Dorman and Sellers, 1989) are biased towards the high end, leading to underestimation of near-surface wind speeds in the NCEP–NCAR reanalysis data set relative to *in situ* measurements.

Near-surface flow as manifest in the two reanalysis data sets for 1958–2001 is thus evaluated in terms of:

1. The spatial variability of 10 m wind speeds. This analysis is focused on qualitative assessment of the degree of correspondence of the mean spatial patterns as manifest in the two data sets.
2. The temporal autocorrelation of wind speeds at grid cells listed in Table I. Temporal autocorrelation is the correlation of successive values in a time series at specified lag intervals; thus, this analysis is focused on assessment of the temporal variability of wind speeds as manifest in the reanalysis data sets. In this analysis we present correlation coefficients for observations of wind speed at lag intervals of 6 h to 8 days.
3. Probability distributions of wind speeds at three grid cells that are coincident or nearly so between the two reanalysis data sets and HadCM3. The empirical cumulative probability distributions are inter-compared and evaluated. The quantitative component of this analysis is based on application of the Kolmogorov–Smirnov (K–S) statistic and test statistics from Stephens (1986). These are conducted under the assumption that wind speeds, particularly over water surfaces, most closely approximate the two-parameter Weibull distribution (Pavia and O'Brien, 1986; Pryor *et al*., 2004) and, hence, that the degree of deviation of the empirical cumulative probability distributions from this may be used as an index of the quality of the reanalysis data. The two-parameter Weibull probability density function is given by

$$p(U) \equiv 1 - \exp\left[-\left(\frac{U}{A}\right)^{k}\right] \qquad \text{for } U \geq 0,\ A > 0,\ k > 0 \tag{2}$$

where k is the dimensionless shape parameter, A is the scale parameter, U represents the wind speed observations, and $p(U)$ is the probability density function.

The cumulative distribution function $P(U)$ is given by

$$P(U) \equiv 1 - \exp\left(\frac{U}{A}\right)^{k} \tag{3}$$

The test for the null hypothesis H_0, that the data set of U comes from the Weibull distribution where A and k are not known *a priori*, is conducted as follows:

1. The time series of U is transformed to give $X(1, \ldots, n)$, where $X(i) = -\log(U(1, \ldots, n))$, and n is the total number of observations.
2. $X(1, \ldots, n)$ are sorted in ascending order.

3. $X(1,\ldots,n)$ is tested to determine whether it is drawn from the extreme-value distribution:

$$P(X) \equiv \exp\left[-\exp\left(-\frac{X-\phi}{\theta}\right)\right] \tag{4}$$

with $\phi = 1/k$, and $\theta = -\log(A)$.

Assuming that k and A, and hence ϕ and θ, are unknown, they are estimated using the maximum likelihood:

$$\theta = \sum_j \frac{X_j}{n} - \frac{\left[\sum_j X_j \exp\left(\frac{-X_j}{\theta}\right)\right]}{\left[\sum_j \exp\left(\frac{-X_j}{\theta}\right)\right]} \tag{5}$$

This is solved iteratively and the result used to determine ϕ:

$$\phi = -\theta \log\left[\sum_j \frac{\exp\left(\frac{-X_j}{\theta}\right)}{n}\right] \tag{6}$$

The results for ϕ and θ are then used in Equation (4) to calculate $Z(1,\ldots,n) = P(X(i), i = 1,\ldots,n)$. $Z(1,\ldots,n)$ are sorted in ascending order and used to calculate the empirical cumulative distribution function (ECDF) statistics (A^2 and W^2):

$$A^2 = -n - \left(\frac{1}{n}\right)\sum_j (2j-1)[\log Z_j + \log(1 - Z_{n+1-j})] \tag{7}$$

$$W^2 = \sum_j [Z_j - (2j-1)]^2 + \frac{1}{12n} \tag{8}$$

$1 \le j \le n$. These are compared against critical values (denoted by A^{2*} and W^{2*}; Stephens, 1986). If $A^2[1 + (0.2/\sqrt{n})] > A^{2*}$ ($A^{2*} = 0.757$ for $\alpha = 0.05$, and $A^{2*} = 1.038$ for $\alpha = 0.01$) or $W^2[1 + (0.2/\sqrt{n})] > W^{2*}$ ($W^{2*} = 0.124$ for $\alpha = 0.05$ and $W^{2*} = 0.175$ for $\alpha = 0.01$) for a given significance level α, then H_0 can be rejected at that level. This approach was evaluated using 100 synthetic Weibull distributions ($n = 1000$) generated as in Pryor *et al.* (2004). For the 100 synthetic data sets, only two were found to result in rejection of H_0.

The test statistics used are reliant on independence of observations in the data series, which is frequently violated in real time series of atmospheric variables (Kristensen *et al.*, 2002). Hence, here, we adjust the sample size used in the K–S test for the lag-1 correlation (von Storch and Zwiers, 1999) and multiply and randomly sample the time series from the reanalysis data sets to draw 100 data sets containing 2000 observations. These are then subjected to the test for fit to a Weibull distribution using the A^2 and W^2 statistics. The selection of the number of samples to contain in each data subset ($n = 2000$) is based on analyses conducted to assess the critical sample size required to generate a stable estimate of the Weibull A and k parameters for a data set that conforms to a Weibull distribution (Pryor *et al.*, 2004).

4. Temporal trends at grid cells that are spatially coincident or nearly so between the two reanalysis data sets and HadCM3 (see Table I). This analysis is focused on assessment of the degree of correspondence of temporal trends in percentiles of the wind speed distributions as manifest in the two reanalysis data sets. The 'trend' is calculated using linear regression:

$$y = mx + c \tag{9}$$

where y is the Xth percentile wind speed in each year, c is the Xth percentile wind speed in 1957, m is the trend term (i.e. the increase or decrease in the Xth percentile wind speed (m s^{-1} $year^{-1}$)) and x is the year since 1957 (Pryor and Barthelmie, 2003). Values are only shown if the 95% confidence intervals on the trend term did not include zero (i.e. the trend term is statistically different to zero).

3.2.2. Results. Mean 10 m wind speeds for 1958–2001, as manifest in NCEP–NCAR and the ECMWF reanalysis data sets, are shown in Figure 3. The largest discrepancy in terms of the mean wind fields is found in southern Norway, where the ECMWF reanalysis indicates mean wind speeds during 1958–2001 below 2.5 m s^{-1} and the NCEP–NCAR reanalysis data show values in excess of 2.5 m s^{-1}. This part of the domain is strongly influenced by the Scandic Mountains, which form the spine of the peninsula on which Sweden and Norway are located and which reach heights of 2469 m above sea level. The differing spatial resolutions of the NCEP–NCAR and ECMWF models and data archiving may manifest differing drag and blocking effects caused by this mountain range. The data sets also differ in terms of the wind speeds in the central Baltic Sea (i.e. over water). These portions of the domain generally exhibit higher wind speeds in the NCEP–NCAR data set than in the ECMWF reanalysis. Since water has a low and dynamic roughness in the models, this may imply higher average near-surface pressure gradients in the NCEP–NCAR reanalysis project and hence higher wind speeds. In general, grid cells in the western portion of the domain (A–F in Table I) exhibit higher means and upper percentiles in the NCEP–NCAR data set. However, this is not uniformly true of all grid cells. For example, ECMWF data from grid cells G and N exhibit higher upper percentile wind speeds

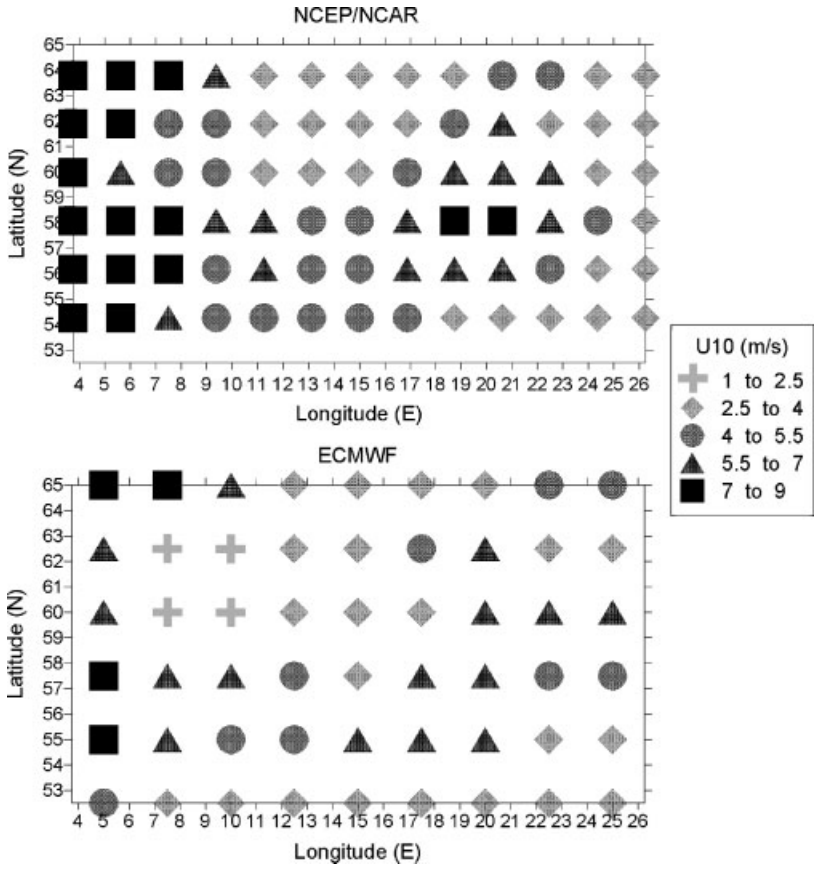

Figure 3. Mean 10 m wind speeds 1958–2001 from the four-times daily data from the NCEP–NCAR and ECMWF reanalysis data sets. The domain is as shown in Figure 1

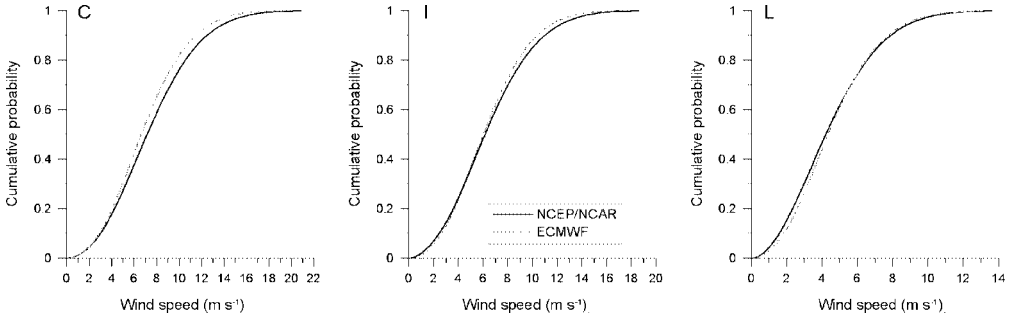

Figure 4. Empirical cumulative distributions (0.1–99.9th percentiles) for three grid cells (C, I and L) from the NCEP–NCAR and ECMWF data for the period 1958–2001

and, as shown in Figure 4, data for grid cell L also exhibit slightly higher 90th percentile wind speeds than the NCEP–NCAR data.

Figure 5 shows the temporal autocorrelation functions calculated using the NCEP–NCAR and ECMWF reanalysis data sets (1958–2001) for the grid cells described in Table I. As shown, the temporal autocorrelation functions are very similar both for individual grid cells and spatially (e.g. higher persistence in the western grid cells). However, there is evidence of a slightly stronger diurnal cycle at the eastern grids in the ECMWF data.

Although the ECDFs from the NCEP–NCAR and ECMWF data sets for 1958–2001 are also qualitatively similar, at the three grid cells shown in Figure 4 the null hypothesis (that the distributions are equal) is rejected by the K–S equality of distributions test at a confidence level in excess of 95%. Also, at grid cell

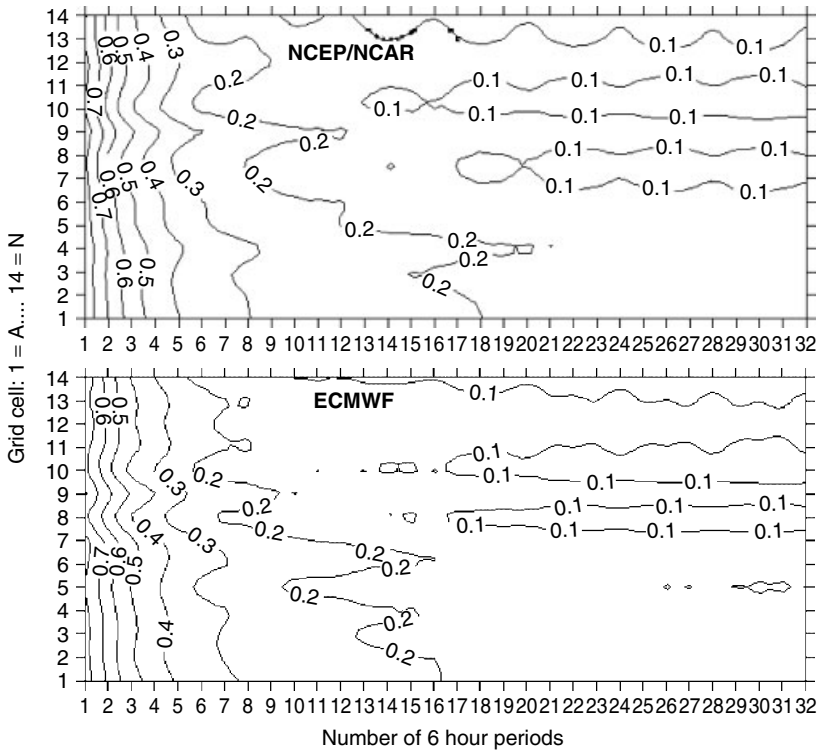

Figure 5. Temporal autocorrelation functions for 6 h data from the NCEP–NCAR and ECMWF reanalysis data sets computed using data from 1958–2001 for the grid cells described in Table I. The contours represent the Pearson correlation for observations at time t with those from $t + n$, where $n = 1$–32, equating to time lags of 6 h to 8 days

C, the mean wind speed differs by approximately 8%, with the NCEP–NCAR data showing a higher mean. At grid cell I, the means differ by approximately 3%, again with NCEP–NCAR being higher. At grid cell L the means differ by less than 2% and, unlike the other grid cells, the ECMWF data exhibit a slightly higher mean wind speed.

As shown in Table II, the reanalysis data sets generally do not conform to a Weibull distribution according to the A^2 and W^2 statistics. The lack of fit to a Weibull distribution may be due to a number of causes, such as mixed forcing of the wind regime, e.g. blending of flow regimes induced by local thermal effects with the prevailing synoptic regime. Accordingly, the 'best' fit is observed in the water-dominated grid cells where synoptic forcing of the wind speeds dominates. Hence, a lack of 'fit' to a Weibull distribution cannot unequivocally be assigned to inaccurate representation of near-surface wind speeds. Nevertheless, it is noteworthy that the analysis implies that the 6 h NCEP–NCAR reanalysis data more closely approximate the distribution that is most commonly used to calculate electricity generation potential in the wind energy industry (Pryor *et al*., 2004).

Figure 6 shows an example of the evolution of the annual probability distributions from the NCEP–NCAR and ECMWF data sets in terms of the annual 10th, 50th and 90th percentiles of the four-times daily wind speeds, and Table I summarizes temporal trends in the annual 90th percentile wind speeds at all common grid cells. Figure 6 illustrates the absence of trends in the lower percentiles that is common to all grid cells. This figure also demonstrates that, in line with analysis of storms in northwest Europe (Alexandersson *et al*., 2000), the highest 90th percentile wind speeds in the southwestern Baltic occurred in the late 1980s and early 1990s and the upper percentiles of the wind speed distribution have subsequently declined in both data sets. Figure 6 and Table I agree with the findings of earlier work (Pryor and Barthelmie, 2003) and emphasize that the latter portion of the C20th was characterized by higher wind speeds, particularly in the southwest of the Baltic region. All grid cells that showed statistically significant wind speed trends showed positive trends in both data sets, although, on average, the trends were smaller in the ECMWF data. It is noteworthy that, whereas there is clear correspondence between the reanalysis data sets in terms of mutual identification of high wind speed years (e.g. 1990), the magnitude of variability and ensemble effect in terms of the wind energy density (Figure 2) is not consistent.

Table II. ECDF statistics for analysis of the degree of fit to a Weibull distribution. The values shown are the number of the 100 randomly selected data sets ($n = 2000$) for which computed A^2 and W^2 statistics indicate the data fail to conform to a Weibull distribution at the 99% confidence level. Data for 1958–2001 reflect the four-times daily data, and the statistics for 1990–2001 are calculated using daily average data

	6 h data: 1958–2001				Daily average data: 1990–2001					
	NCEP–NCAR		ECMWF		NCEP–NCAR		ECMWF		HadCM3	
Grid cell	A^2	W^2	A^2	W^2	A^2	W^2	A^2	W^2	A^2	W^2
A	20	12	2	4	97	95	100	100	100	98
B	8	3	3	0	100	99	95	69	88	78
C	8	1	5	4	100	95	100	100	100	98
D	21	12	5	5	100	100	100	100	99	88
E	32	11	95	75	67	39	100	100	100	95
F	0	0	43	39	100	100	100	100	100	100
G	19	17	1	1	100	99	100	99	99	98
H	8	2	88	84	100	100	100	100	100	100
I	25	9	3	3	100	99	100	100	100	100
J	6	5	55	48	100	100	100	100	100	100
K	22	7	84	71	100	100	100	100	100	100
L	2	3	15	15	100	100	100	100	100	100
M	15	7	95	84	100	100	100	100	99	100
N	2	3	89	84	100	100	100	100	100	100

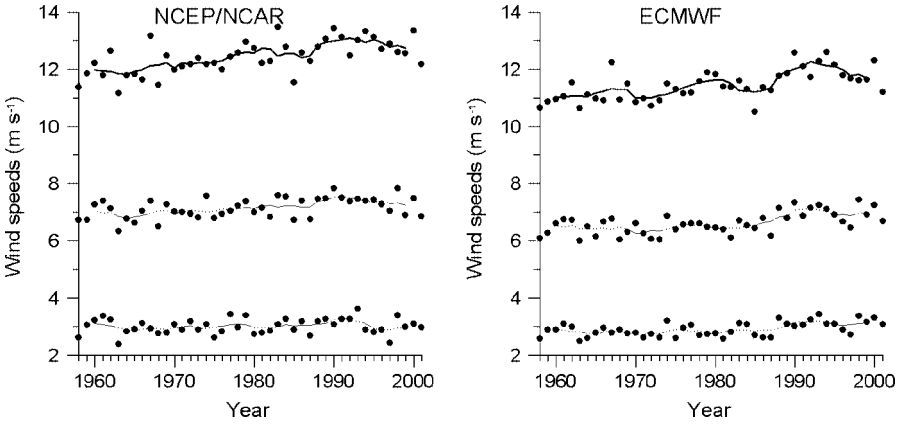

Figure 6. Annual 10th, 50th and 90th percentile wind speeds for grid cell C (western Denmark). Also shown are lines depicting a 5 year running mean

In summary, the two reanalysis data sets are broadly consistent in terms of the absolute magnitude of wind speeds, probability distributions, spatial patterns and trends; but there are discrepancies that may be due to:

1. Differences in the data assimilated into the two reanalysis models.
2. Differences in the surface parameterizations used in the models. Surface roughness and topography may differ both as a result of differing spatial resolution and data source.
3. Differences in the pressure gradients manifest in the models resulting from, for example, differences in storm tracks.

Differentiating between these is the subject of ongoing research.

4. DEVELOPMENT OF WIND-ENERGY PROJECTIONS BASED ON HADCM3

4.1. Evaluation of AOGCM simulation: comparison of the reanalysis data sets and HadCM3 simulations for 1990–2001

4.1.1. Methods. AOGCMs exhibit greatest accuracy at large scales and long averaging periods (Houghton *et al*., 2001). Although research has been conducted to generate prognostic storm frequencies and magnitude (e.g. Debernard *et al*., 2002), few studies have evaluated the ability of AOGCMs to reproduce the distribution of near-surface flow, which, within the mid-latitudes, is largely determined by pressure gradients. These pressure gradients, in turn, are a function of the prevailing synoptic-scale circulation patterns and interaction with local topographic and land cover conditions. The accurate simulation of near-surface wind speeds thus requires accurate performance of the AOGCM across a range of scales and accuracy of boundary conditions.

Prior to use of HadCM3 simulation output to develop wind energy projections over the Baltic, it is important to evaluate the performance of the HadCM3 with respect to the validity of phenomena during the period of overlap between the reanalysis data set and the AOGCM transient simulation (i.e. 1990–2001). Hence, we evaluate the model relative to the two reanalysis data sets with respect to the following model performance parameters:

1. Mean wind speed fields derived from daily data and the spatial correlations of data from model grid cells.
2. The temporal autocorrelation functions of daily wind speeds at grid cells that are coincident (or nearly so) between the two reanalysis data sets and HadCM3 (see Table I). The persistence of flow has important consequences for the feasibility of harnessing wind energy, owing to the influence on predictability (Pryor and Barthelmie, 2002), but it is used here primarily to assess the tendency of the models to exhibit day-to-day variability primarily associated with the synoptic scale.

3. Comparisons of wind speed probability distributions for individual grid cells and for all common grid cells.

The quantitative aspects of the comparison undertaken in (2) (analysis of the temporal autocorrelation) and (3) (analysis of the ECDFs) use the techniques described in Section 3.2.

4.1.2. Results. Figure 7 shows the mean daily 10 m wind speed fields from HadCM3 and the reanalysis data set for 1990–2001. As in Figure 3, the largest discrepancy in terms of the mean wind fields is found in southern Norway, where, as in the case of the longer data set, the ECMWF reanalysis indicates mean wind speeds during 1990–2001 below 2.5 m s^{-1} and both HadCM3 and the NCEP–NCAR reanalysis data

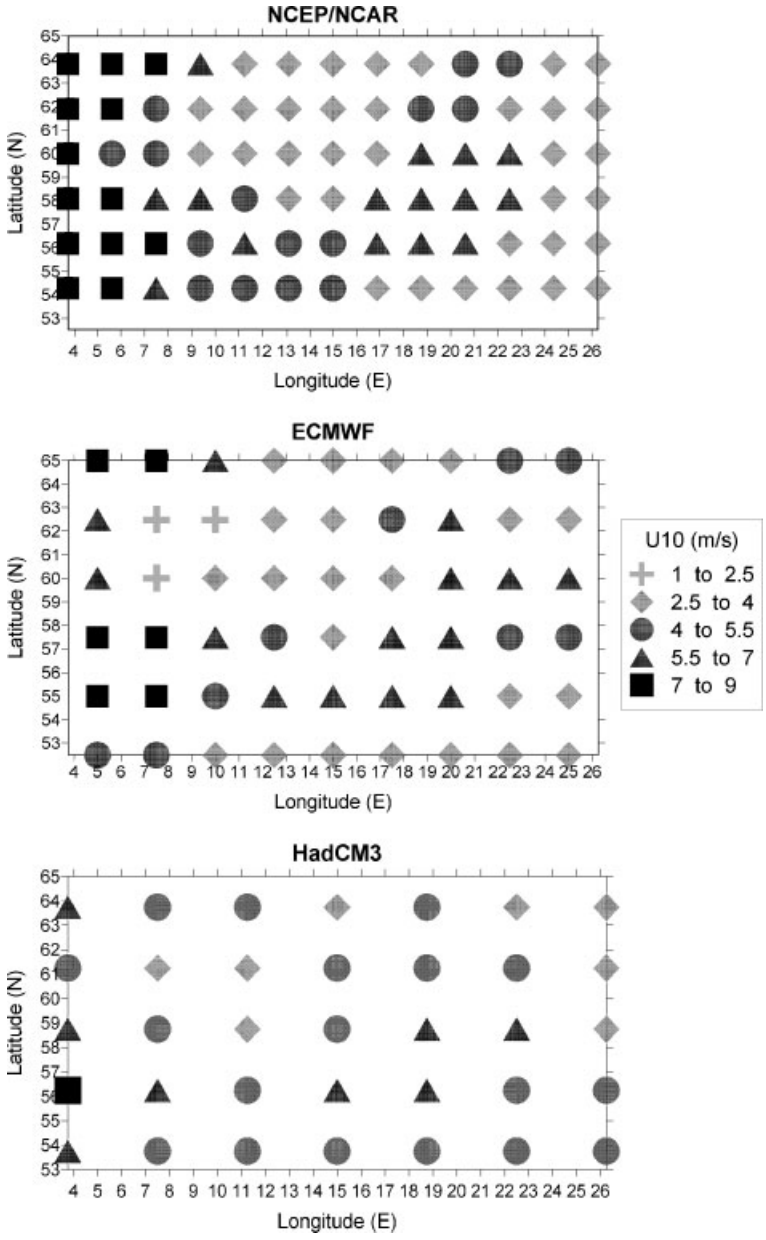

Figure 7. Mean of the daily mean 10 m wind speed from HadCM3 and the two reanalysis data sets for the period 1990–2001. The domain is as shown in Figure 1

show values in excess of 2.5 m s^{-1}. On average, 10 m data from the HadCM3 correctly captures the spatial pattern of mean wind speeds, but HadCM3 simulated wind speeds are typically lower in absolute magnitude, particularly in Norway and also over the interior of the Baltic Sea.

Figure 8 shows the correlation coefficients for daily wind speeds at the grid cells listed in Table I. As shown, the spatial decay of associations from all three data sets is (i) largest for the northern grids and (ii) stronger for changing latitude than longitude. It may be notable that the reanalysis data sets exhibit small negative correlations between easterly and westerly grid cells that may be related to storm tracking, but this feature is not observed in the time series from HadCM3.

Figure 9 shows the temporal autocorrelation functions for daily wind speeds during 1990–2001 from NCEP–NCAR, ECMWF and HadCM3. As shown, there is some evidence that HadCM3 exhibits higher persistence of wind speeds, particularly in the west of the region at lags beyond 1 day, which may be taken as evidence that HadCM3 underestimates the variance of wind speeds, or, alternatively stated, that HadCM3 underestimates the variability inherent in flow over the study region.

Figure 10 shows the ECDFs for daily wind speeds for 1990–2001 for three sample grid cells for the NCEP–NCAR, ECMWF and HadCM3 simulations. It might be expected that as the spatial scale represented by a given wind speed time series increases there will be a steepening of the ECDF (or a narrowing of the probability distribution), i.e. a decrease in the difference between lower and upper percentiles. However, as shown in Figure 10, HadCM3 shows relatively good correspondence to the reanalysis data for the lower percentiles (low wind speeds), but it underestimates the higher percentiles. Thus, this analysis offers supporting evidence to the assertion made on the basis of the temporal autocorrelation, that HadCM3 underestimates the variability of wind speeds, and most specifically the upper tail of the wind speed distribution. On average, 10 m data from HadCM3 correctly capture the spatial pattern of mean wind speeds, but, as shown in Figure 7, HadCM3 simulated wind speeds are lower in absolute magnitude in the northwest and southwest of the domain than those from the reanalysis data sets. Further work is required to clarify whether the discrepancies between the HadCM3 and reanalysis data in terms of temporal and spatial correlations and probability distributions of daily wind speeds are due to the differing spatial resolutions of the models and data archives or a dynamical cause (e.g. differences in the tracking or intensity of synoptic-scale phenomena in the models). As a first analysis of the importance of the spatial grid resolution/data aggregation, Figure 10 presents a comparison of the cumulative probability distribution for data from all common grid cells. As shown in Figure 10, the correspondence of wind speeds improves with scale, but HadCM3 appears to underestimate wind speeds over the domain as a whole across the higher percentiles of the probability distribution, indicating a potential systematic bias in HadCM3 that may reflect spatial scale or a weakness in simulation of pressure gradients. Table II shows the results of analyses of the ECDFs for the fit to the Weibull distribution for 1990–2001. As shown, the ECDFs of daily mean wind speed time series from HadCM3, like those from the reanalysis data, show substantial deviations from Weibull distributions.

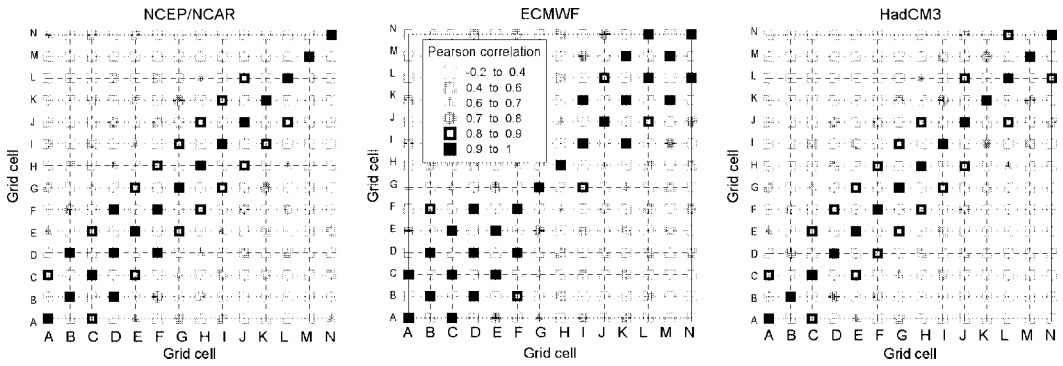

Figure 8. Spatial correlations of daily wind speeds from common grid cells (Table I) in NCEP–NCAR, ECMWF and HadCM3 for data from 1990–2001

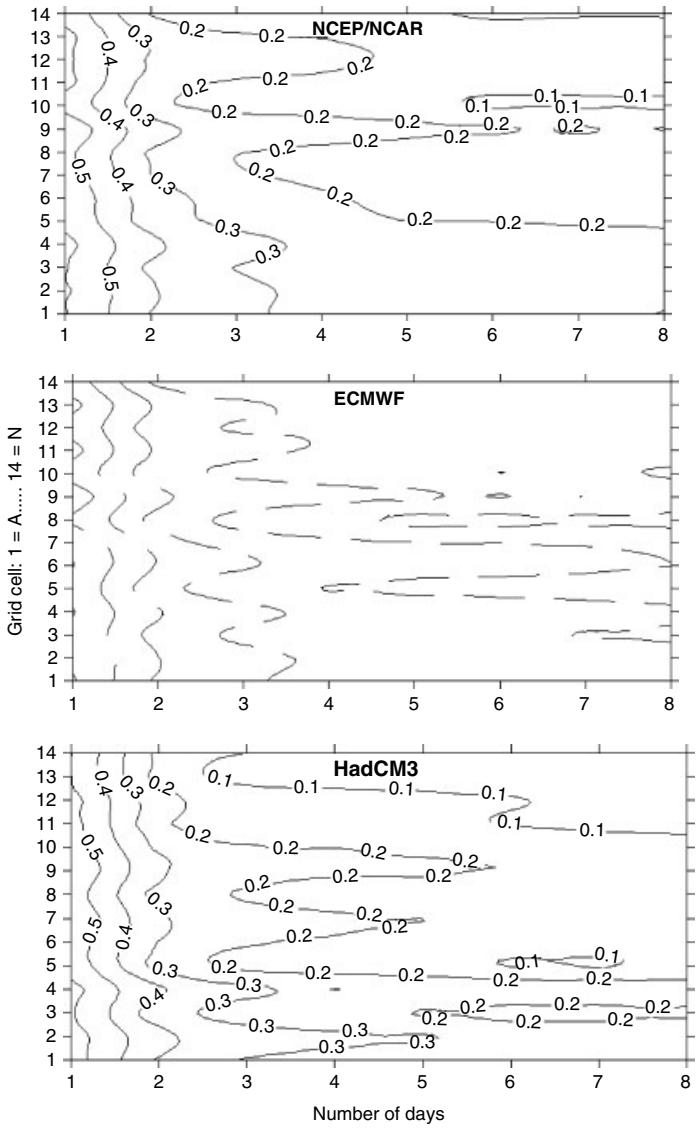

Figure 9. Temporal autocorrelation functions for daily average wind speed data from the NCEP–NCAR and ECMWF reanalysis data sets and HadCM3 computed using data from 1990–2001 for the grid cells described in Table I. The contours represent the Pearson correlation for observations at time t with those from $t + n$, where $n = 1$–8, equating to time lags of 1 to 8 days

4.2. Projected wind indices based on HadCM3

4.2.1. Methods. As shown above there is some evidence of an apparent offset in mean absolute wind speeds between those simulated by HadCM3 and those in the reanalysis data set for the period of overlap (1990–2001). However, the spatial variability of wind speeds and some degree of the variability around the mean at individual grid cells do seem to be reproduced by HadCM3. Thus, it is deemed reasonable to use the normalized wind index to calculate prognostic wind energy estimates using the daily wind speeds from HadCM3 for the C21st to provide a first assessment of likely changes in wind energy availability in the Baltic region. As described above, use of wind indices reduces the impact of biases in the HadCM3 simulated wind speeds and also represents a metric that is well known to the wind-energy community. Hence, annual wind indices were calculated for each HadCM3 grid cell using Equation (1) and a normalization period of 1990–2001.

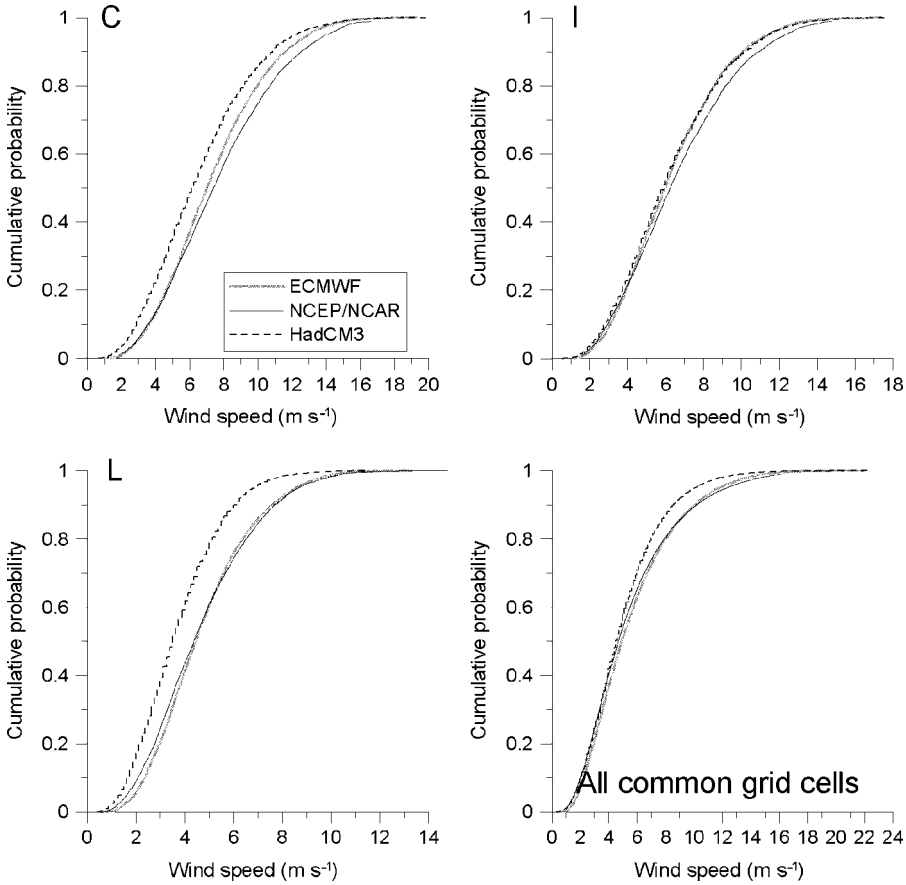

Figure 10. Comparison of ECDF (0.1–99.9th percentiles) from the HadCM3 and the NCEP–NCAR and ECMWF reanalysis daily average 10 m wind speeds for three selected grid cells and using data from all common grid cells for the period 1990–2001 (see Table I)

4.2.2. Results. Figure 11 shows the annual wind indices for the C21st for grid cells C, I and L calculated using daily wind speeds from HadCM3. For a normalization period of 1990–2001 the mean annual wind index for grid cell C for 1990–2099 is 98%, for grid cell I it is 99% and for grid cell L it is 103%. These values are compared with mean annual wind indices calculated using the reanalysis data from 1958–2001 in Table III. As shown in Figure 11 and Table III, there is evidence of a weak downward trend in the annual wind index in grid C during C21st but a tendency towards increased wind indices in grid cell L, which may imply more northerly tracking of synoptic systems or increased frequency of blocking high situations (Pryor and Barthelmie, 2003). The mean wind index for grid cell C for the C21st is higher than that computed for 1958–2001 from the reanalysis data (Table III), but still slightly below 100. The inference from Figure 11 is that the 1990–2001 period exhibited atypically high wind speeds over Denmark in both a historical and prognostic context. This projection implies coming decades will exhibit a wind energy climatology for Denmark that is more similar to that which characterized the 1990s than the 1958–2001 period, but that the wind energy density will subsequently decline. Figure 2 indicates that the northeast of the Baltic also experienced atypically windy conditions during the later portion of the 1980s and the 1990s, but the preliminary prognostic wind index for grid cell L (and other grid cells in the northeast of the Baltic) implies the C21st will be characterized by a larger average wind energy resource than either the 1990–2001 or 1958–2001 periods (Table III).

There are a number of caveats that should be applied to these findings:

1. The normalization inherent in calculation of the wind indices reduces the impact of the offset of wind

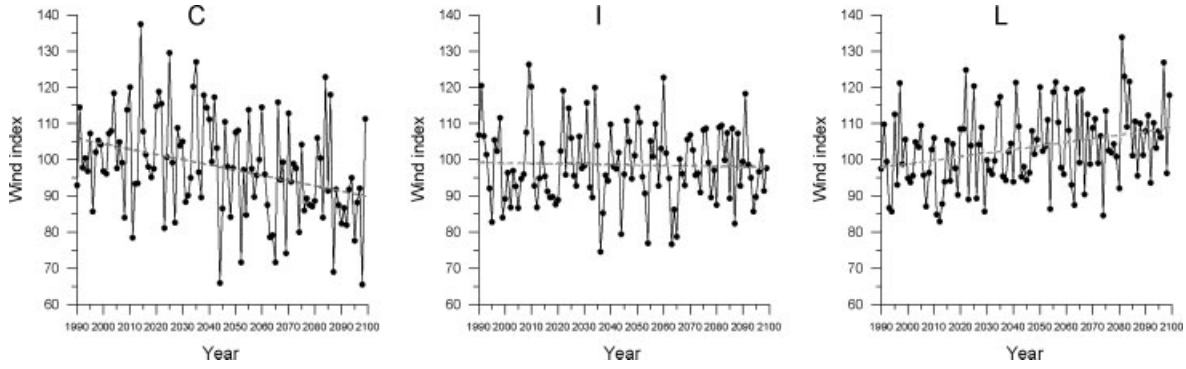

Figure 11. Annual wind indices for grid cells C, I and L calculated using daily wind speeds as simulated by HadCM3 and a normalization period of 1990–2001. The best-fit lines show the linear trend derived from regression of annual mean wind index on year

Table III. Mean (and standard deviation) of annual wind indices from 1958–2001 (reanalysis data) and 1990–2099 (HadCM3) for grid cells C, I and L

	Mean (standard deviation) wind index		
	Grid cell C	Grid cell I	Grid cell L
NCEP–NCAR: 1958–2001 ($n = 44$)	91 (11)	92 (11)	91 (14)
ECMWF: 1958–2001 ($n = 44$)	89 (12)	92 (11)	93 (17)
HadCM3: 1990–2099 ($n = 110$)	98 (14)	99 (11)	103 (11)

speeds simulated by HadCM3 relative to the reanalysis data sets, but the finding is still dependent on the accuracy of HadCM3 with respect to the variability and range of wind speeds. As shown in Section 4.1, there is evidence that HadCM3 underestimates this variability. Nevertheless, there is considerable evidence that GCMs are most robust at spatial scales beyond the individual grid cell, and the finding of differential projected trends in the southwest and northeast of the Baltic is supported by analysis of data from multiple HadCM3 grids.

2. The simulated wind speed data series treated here are characteristic of large spatial scales, and although the synoptic scale dominates interannual variability of wind speeds, sub-synoptic spatial scales determine the actual wind resource at any given wind farm.
3. The results presented here represent annual averages and are based on daily wind speeds, so no inferences can be made with respect to seasonal or diurnal changes in wind energy availability.

5. CONCLUDING REMARKS

Over the period 1958–2001, data from two reanalysis data sets (NCEP–NCAR and ECMWF) exhibit a high degree of coherence over the Baltic in terms of wind speed statistics (spatial patterns, wind speed distributions and temporal trends and autocorrelations). Over the majority of the Baltic region, upper percentile wind speeds and, hence, wind energy density were higher towards the end of the data record than at the beginning, due in part to increased prevalence of westerly flow regimes and positive phase NAO. The largest discrepancies between the data sets are that the ECMWF data at a $2.5^\circ \times 2.5^\circ$ resolution exhibit lower wind speeds, particularly over southern Norway, relative to the NCEP–NCAR data (which have a resolution of approximately 1.875°), and the interannual variability and particularly the timing of maximum annual wind energy density exhibit some differences (both for individual grid cells and spatially). For the 1990–2001 period the reanalysis data sets also exhibit commonalities with data from HadCM3 simulations, although,

perhaps because the former assimilate data, there are greater discrepancies between the AOGCM and the reanalysis data than between the reanalysis products. For example, HadCM3 tends to overpredict the temporal autocorrelation and spatial correlation of daily wind speeds.

Observed changes in flow regimes during the second half of C20th over the Baltic have important consequences for choice of normalization period for calculation of wind indices. For example, using a normalization period of 1987–98 (as in the Danish wind index) leads to overestimation of the wind energy index in western Denmark relative to 1958–2001 by approximately 10%. To address whether the trend towards greater prevalence of higher wind speeds in the latter portion of the C20th will be maintained in the future, we provide a first prognosis of annual wind indices from the HadCM3 AOGCM. The results indicate that the C21st will be similar to the 1958–2001 period with respect to the wind energy density. There is evidence of a weak downward trend in the annual wind index in grid cells from the southwest of the Baltic during the C21st but a tendency towards increased wind indices in grid cells from the northeastern Baltic, which may be linked to changes in the synoptic climate and larger scale teleconnection indices. These results are preliminary and it should be emphasized that, as documented herein, the reanalysis data sets from NCAR–NCEP and ECMWF differ in terms of the spatial fields and empirical cumulative probability distributions at individual grid cells and that these data differ from the simulated fields generated by HadCM3. Future work will focus on defining causes of the discrepancies between the reanalysis data sets, undertaking further evaluation of AOGCM simulations and development and application of novel downscaling techniques to provide more robust wind speed and wind energy prognoses.

This research contributes to the overarching objective of understanding the regional structure and manifestations of climate change. Although this paper focuses on implications of a changing wind climate on wind energy resource assessment and harnessing, there are a number of other implications of changing flow regimes, ranging from storm surge magnitude and frequency (Bijl, 1997), the wave climate and coastal defence (Bouws *et al*., 1996; The WASA Group, 1998), and building construction (Sanders and Phillipson, 2003).

ACKNOWLEDGMENTS

The NCEP–NCAR reanalysis products are from http://www.cdc.noaa.gov/cdc/reanalysis/. ECMWF reanalysis data are available from http://www.ecmwf.int/research/era/. The Danish wind energy index is available from http://www.emd.dk/. The HadCM3 output was obtained from the Climate Impacts LINK Project (DERFA contract EPG 1/1/124) on behalf of the Hadley Centre and UK Meteorological Office. Financial support was provided by 'Impacts of Climate Change on Renewable Energy Sources and their Role in the Energy System: 2003–2006' project funded by Nordic Energy Research (under the Nordic Council of Ministers) and the 'Stormaalepark' project funded by the Danish PSO-F&U program. JTS also acknowledges a Dissertation Year Research Fellowship from Indiana University.

The computational component of this research was made possible by grants to Indiana University from IBM Inc. (Shared University Research) and the National Science Foundation (0116050).

REFERENCES

Alexandersson H, Tuomenvirta H, Schmith T, Iden K. 2000. Trends of storms in NW Europe derived from an updated pressure data set. *Climate Research* **14**: 71–73.

Bijl W. 1997. Impact of a wind climate change on the surge in the southern North Sea. *Climate Research* **8**: 45–59.

Bouws E, Jannick D, Komen G. 1996. The increasing wave height in the North Atlantic Ocean. *Bulletin of the American Meteorological Office* **77**: 2275–2277.

Debernard J, Saetra O, Roed L. 2002. Future wind, wave and storm surge climate in the northern North Atlantic. *Climate Research* **23**: 39–49.

Dorman JL, Sellers P. 1989. A global climatology of albedo, roughness length and stomatal resistance for atmospheric general circulation models as represented by the Simple Biosphere model (SiB). *Journal of Applied Meteorology* **28**: 833–855.

Frank HP, Mann J. 2001. *50 year return wind around Denmark from global reanalysis data*. Wind energy for the new millennium. In *2001 European Wind Energy Conference and Exhibition (EWEC '01)*, Copenhagen, DK. WIP Renewable Energies: München.

Geng Q, Sugi M. 2001. Variability of the North Atlantic cyclone activity in winter analyzed from NCEP–NCAR reanalysis data. *Journal of Climate* **14**: 3863–3873.

Gerstengarbe F, Werner PC. 1999. Katalog der Grosswetterlagen Europas nach Paul Hess and Helmuth Brezokwsky (1881–1998). Potsdam Institute for Climate Impact Research, Potsdam, Germany.

Greatbach RJ. 2000. The North Atlantic oscillation. *Stochastic Environmental Research and Risk Assessment* **14**: 213–242.
Hastenrath S, Greischar L. 2001. The North Atlantic oscillation in the NCEP–NCAR reanalysis. *Journal of Climate* **14**: 2404–2413.
Hines K, Bromwich D, Marshall G. 2000. Artificial surface pressure trends in the NCEP–NCAR reanalysis over the Southern Ocean and Antarctica. *Journal of Climate* **13**: 3940–3952.
Houghton JT, Ding Y, Gmggs DJ, Noguer M, van der Linden PJ, Dai X, Maskell K, Johnson CA (eds). 2001. *Climate Change 2001: The Scientific Basis*. Cambridge University Press: Cambridge, UK.
Johns TC, Carnell RE, Crossley JF, Gregory JM, Mitchell JFB, Senior CA, Tett SFB, Wood RA. 1997. The second Hadley Centre coupled ocean–atmosphere GCM: model description, spinup and validation. *Climate Dynamics* **13**: 103–134.
Kalnay E, Cai M. 2003. Impact of urbanization and land-use change on climate. *Nature* **423**: 528–531.
Kalnay E, Kanamitsu M, Kistler R, Collins W, Deaven D, Gandin L, Iredell M, Saha S, White G, Woollen J, Chelliah M, Zhu Y, Chelliah M, Ebisuzaki W, Higgins W, Janowiak J, Mo KC, Ropelweski C, Wang J, Leetmaa A, Reynolds R, Jenne R, Joseph D. 1996. The NCEP/NCAR 40 reanalysis project. *Bulletin of the American Meteorological Society* **77**: 437–471.
Kistler R, Kalnay E, Collins W, Saha S, White G, Woollen J, Chelliah M, Ebisuzaki W, Kanamitsu M, Kousky V, van den Dool H, Jenne R, Fiorino M. 2001. The NCEP–NCAR 50 year reanalysis: monthly mean CD-ROM and documentation. *Bulletin of the American Meteorological Society* **82**: 247–267.
Kristensen L, Kirkegaard P, Mann J. 2002. Sampling statistics of atmospheric observations. *Wind Energy* **5**: 301–313.
Marshall GJ. 2002. Trends in Antarctic geopotential height and temperature: a comparison between radiosonde and NCEP–NCAR reanalysis data. *Journal of Climate* **15**: 659–674.
Marshall J, Kushnir Y, Battisti D, Chang P, Czaja A, Dickson R, Hurrell J, McCartney M, Saravanan R, Visbeck M. 2001. North Atlantic climate variability: phenomena, impacts and mechanisms. *International Journal of Climatology* **21**: 1863–1898.
Mengelkamp H. 1999. Wind climate simulation over complex terrain and wind turbine energy output estimation. *Theoretical and Applied Climatology* **63**: 129–139.
Nakicenovic N, Swart R (eds). 2000. *Special Report on Emissions Scenarios*. Cambridge University Press: Cambridge, UK.
Pavia EG, O'Brien JJ. 1986. Weibull statistics of wind speed over the ocean. *Journal of Climate and Applied Meteorology* **25**: 1324–1332.
Pope V, Gallani M, Rowntree P, Stratton R. 2000. The impact of new physical parameterizations in the Hadley Centre climate model: HadAM3. *Climate Dynamics* **16**: 123–146.
Pryor SC, Barthelmie RJ. 2002. Statistical analysis of flow characteristics in the coastal zone. *Journal of Wind Engineering and Industrial Aerodynamics* **90**: 201–221.
Pryor SC, Barthelmie RJ. 2003. Long term trends in near surface flow over the Baltic. *International Journal of Climatology* **23**: 271–289.
Pryor SC, Nielsen M, Barthelmie RJ, Mann J. 2004. Can satellite sampling of offshore wind speeds realistically represent wind speed distributions? Part II. quantifying uncertainties associated with sampling strategy and distribution fitting methods. *Journal of Applied Meteorology* **43**: 739–750.
Sailor D, Hu T, Li X, Rosen J. 2000. A neural network approach to local downscaling of GCM output for assessing wind power implications of climate change. *Renewable Energy* **19**: 359–378.
Sanders CH, Phillipson MC. 2003. UK adaptation strategy and technical measures: the impacts of climate change on buildings. *Building Research and Information* **31**: 210–221.
Schoof JT, Pryor SC. 2003. Evaluation of the NCEP–NCAR reanalysis in terms of synoptic scale phenomena: a case study from the Midwestern USA. *International Journal of Climatology* **23**: 1725–1741.
Serreze MC, Carse F, Barry RG. 1997. Icelandic low cyclone activity: climatological features, linkages with the NAO and relationships with recent changes in the Northern Hemisphere circulation. *Journal of Climate* **10**: 453–464.
Simmons AI, Gibson JK. 2000. The ERA-40 Project Plan. UK Meteorological Office, UK. http://www.ecmwf.int/publications/library/do/references/list/192. [Last accessed 6 March 2005].
Smith SD, Legler D, Verzone K. 2001. Quantifying uncertainties in NCEP reanalyses using high-quality research vessel observations. *Journal of Climate* **14**: 4062–4072.
Stephens MA. 1986. Tests based on EDF statistics. In *Goodness-of-Fit Techniques*, D'Agostino RB, Stephens MA, (eds). Marcel Dekker: New York; 97–193.
Stratton RA. 1999. A high resolution AMIP integration using the Hadley Centre model HadAM2b. *Climate Dynamics* **15**: 9–28.
The WASA Group. 1998. Changing waves and storms in the northeast Atlantic. *Bulletin of the American Meteorological Society* **79**: 741–760.
Trenberth KE, Stepanik DP. 2002. A pathological problem with NCEP reanalysis in the stratosphere. *Journal of Climate* **15**: 690–695.
Ulbrich U, Christoph M. 1999. A shift of the NAO and increasing storm track activity over Europe due to anthropogenic greenhouse gas forcing. *Climate Dynamics* **15**: 551–559.
Von Storch H, Zwiers FW. 1999. *Statistical Analysis in Climate Research*. Cambridge University Press: Cambridge, UK.

